Small Conductance Potassium Channels Cause an Activity-Dependent Spike Frequency Adaptation and Make the Transfer Function of Neurons Logarithmic

Jutta Engel,* Howard A. Schultens,** and Detlev Schild**
*Physiologisches Institut II, Universität Tübingen, Roentgenweg 11, D-72076 Tübingen, Germany, and **Physiologisches Institut, Universität Göttingen, D-37073 Göttingen, Germany

ABSTRACT We made a computational model of a single neuron to study the effect of the small conductance (SK) Ca^{2+}-dependent K^+ channel on spike frequency adaptation. The model neuron comprised a Na^+ conductance, a Ca^{2+} conductance, and two Ca^{2+}-independent K^+ conductances, as well as a small and a large (BK) Ca^{2+}-activated K^+ conductance, a Ca^{2+} pump, and mechanisms for Ca^{2+} buffering and diffusion. Sustained current injection that simulated synaptic input resulted in a train of action potentials (APs) which in the absence of the SK conductance showed very little adaptation with time. The transfer function of the neuron was nearly linear, i.e., both asymptotic spike rate as well as the intracellular free Ca^{2+} concentration ($[Ca^{2+}]_i$) were approximately linear functions of the input current. Adding an SK conductance with a steep nonlinear dependence on $[Ca^{2+}]_i$ (Leinders and Vijverberg, 1992. *Pflügers Arch.* 422:223–232; Köhler, Hirschberg, Bond, Kinzie, Marrion, Maylie, and Adelman. 1996. *Science.* 273:1709–1714) caused a marked time-dependent spike frequency adaptation and changed the transfer function of the neuron from linear to logarithmic. Moreover, the input range the neuron responded to with regular spiking increased by a factor of 2.2. These results can be explained by a shunt of the cell resistance caused by the activation of the SK conductance. It might turn out that the logarithmic relationships between the stimuli of some modalities (e.g., sound or light) and the perception of the stimulus intensity (Fechner's law) have a cellular basis in the involvement of SK conductances in the processing of these stimuli.

INTRODUCTION

Ca^{2+}-dependent K^+ channels are widely distributed in the brain. This class of K^+ channels counteracts neuronal depolarization in a Ca^{2+}-dependent fashion. There are at least two large subfamilies of Ca^{2+}-dependent K^+ channels that differ in single channel conductance, pharmacology, and most importantly, in their activation characteristics: the large conductance Ca^{2+}-dependent K^+ channel (BK channel) opens depending on both membrane potential and $[Ca^{2+}]_i$ (Barret et al., 1982; Blatz and Magleby, 1987; McManus and Magleby, 1988) whereas the small conductance (SK) Ca^{2+}-dependent K^+ channel is voltage-insensitive (Blatz and Magleby, 1986, 1987; Leinders and Vijverberg, 1992; Köhler et al., 1996). Thus BK channels are activated during the repolarizing phase of the action potential and rapidly deactivate close to the resting potential, while SK channels stay open as long as $[Ca^{2+}]_i$ is sufficiently elevated.

Spike frequency adaptation is a common phenomenon throughout the nervous system (Hille, 1992). It means that a steady stimulus current induces a firing pattern in a neuron that gradually changes from high to low frequency firing or that firing eventually stops because of increasing afterhyperpolarizations. There is accumulating evidence that the SK Ca^{2+}-dependent K^+ channels are responsible for afterhyperpolarizations that have been observed in many neurons, including hippocampal CA1 pyramidal cells (Lancaster and Nicoll, 1987), layer II/III neocortical pyramidal cells (Zhou and Hablitz, 1996), and thalamic reticular neurons (Bal and McCormick, 1993). Because opening of SK channels depends on elevated $[Ca^{2+}]_i$ only, they may stay open between subsequent spikes, partially shunt the membrane resistance, and thereby delay subsequent spikes.

Spike frequency adaptation to an external stimulus is observed in most sensory systems. Sensory adaptation can be based on a variety of mechanisms among which SK channels may play a prominent role. In the olfactory system, for example, SK channels are expressed in the receptor neurons (Schild, 1989), in mitral cells of the olfactory bulb (Wang et al., 1996), and in pyramidal cells of the olfactory cortex (Köhler et al., 1996).

In conjunction with the phenomenon of spike frequency adaptation, transfer functions, i.e., the relationship between input (injected current) and output (adapted spike rate) have been determined for different types of neurons. Linear transfer functions have been described for cortical neurons of the pyramidal tract (Koike et al., 1970) and for visual cortex pyramidal neurons (Mason and Larkman, 1990). In contrast, nonlinear transfer functions with a convex (logarithmic-like) shape have been found in hippocampal CA1 pyramidal cells (Madison and Nicoll, 1984; Lanthorn et al., 1984), in pyramidal neurons of the somatosensory cortex (Connors et al., 1988), and in neocortical pyramidal neurons (Avoli and Olivier, 1989).

Received for publication 17 July 1998 and in final form 17 November 1998.
Address reprint requests to Dr. Detlev Schild, Abt. Mol. Neurophysiologie der Universität Göttingen, Humboldtallee 23, D-37073 Göttingen, Germany. Tel.: ++49-551-39 5915; Fax: ++49-551-39 5923; E-mail: sd@neuro-physiol.med.uni-goettingen.de.

0006-3495/99/03/1310/10 $2.00

Here we investigate the effect of the SK conductance on the adaptation behavior of a neuron. We then determine the type of its transfer functions (steady-state spike rate and $[Ca^{2+}]_i$ vs. input current, respectively) in a computer model. Finally, we suggest that the activity-dependent changes in $[Ca^{2+}]_i$ together with the nonlinear $[Ca^{2+}]$-dependence of SK channels constitute a negative feedback system that leads to a logarithmic transfer function of single neurons.

METHODS

Simulations were performed using the NEURON simulator, version 3.1.0 (Hines, 1993) on a Pentium PC under LINUX. The integration time step was 25 μs.

Electrotonic properties and resting membrane potential

The simplified model neuron consisted of a cylindrical soma and three cylindrical unbranched dendrites. Diameters and lengths were (in μm) 9 and 14 for the soma, 1.5 and 400 for the primary dendrite, and 1 and 600 for the two identical secondary dendrites, respectively. Total membrane area amounted to 6051 μm^2 and membrane capacity to 60.5 pF assuming a specific membrane capacity of 1 $\mu F/cm^2$. A small persistent K^+ conductance underlying the resting membrane conductance (see below) was set to 1.26 10^{-4} S/cm^2 for the soma and to a 10-fold lower value for the dendrites and resulted in an input resistance of 0.81 GΩ and a time constant of 50 ms for the neuron. The cytosolic resistance was set to 35 Ω-cm and the temperature to 20°C.

The persistent K^+ conductance at rest set the resting membrane potential to the potassium equilibrium potential $E_K = -95$ mV. Background synaptic activity was simulated by injecting a continuous current of 35 pA into the soma that shifted the resting potential to -71 mV. Synaptic activity was generally simulated by current injection in the soma because lowpass filtering by the electrically compact dendrites could be neglected in the steady state.

Membrane conductances and Ca^{2+}-dependent mechanisms

The general approach of modeling ionic conductances was based on a Hodgkin-Huxley-type formalism (Hodgkin and Huxley, 1952). The specific conductance g (given in S/cm^2) of ion species i, g_i, is described by the maximum conductance $g_{i,max}$ times the probability of finding a certain number (p) of voltage-dependent activation gates $m(U, t)$ open and a certain number (q) of inactivation gates $h(U, t)$ not closed:

$$g_i = g_{i,max} m^p h^q \quad (1)$$

The current density for ion species i is

$$i_i = g_i(U - E_i) \quad (2)$$

with U being the actual membrane potential and E_i the equilibrium potential of ion species i. The kinetics of the state variable m is described by the first-order differential equation (idem for h)

$$dm/dt = (m_\infty - m)/\tau_m = \alpha_m(1 - m) - \beta_m m \quad (3)$$

In the classic Hodgkin-Huxley scheme the gate rate functions α_m and β_m can be determined by the steady-state gate opening

$$m_\infty = \alpha_m/(\alpha_m + \beta_m) \quad (4)$$

and the time constant of gate relaxation

$$\tau_m = 1/(\alpha_m + \beta_m). \quad (5)$$

As activation and inactivation are not independent in real ion channels (Armstrong, 1992), we often used values for m_∞, h_∞, τ_m, and τ_h that deviate from the scheme for the gate rate functions.

Using the units mV, ms, mM, S/cm^2 for voltage (U), time, concentration, and specific conductance, respectively, we modeled the following specific processes (Fig. 1):

1. Na^+ current I_{Na} (derived from the Na^+ current in olfactory receptor cells; Schild, 1989) with

$$g_{Na} = g_{Na,max} m^3 h$$

and

$$m_\infty = 1/(1 + \exp(-(U + 40)/8))$$

$$\tau_m = 0.2/(1 + 0.0025\,(U + 50)^2) + 0.02$$

$$h_\infty = 1/(1 + \exp((U + 65)/5.6))$$

$$\tau_h = 2/(1 + 0.0009\,(U + 60)^2)$$

$$E_{Na} = 55 \text{ mV}$$

2. Slowly activating K^+ current I_{Ks} with

$$g_{Ks} = g_{Ks,max} m$$

and

$$m_\infty = (1 - 0.02)/(1 + \exp((-(U + 5)/12)) + 0.02$$

$$\tau_m = 10$$

$$E_K = -95 \text{ mV}$$

3. Fast-activating and -inactivating K^+ current I_{Kf} (derived from the transient K^+ current in olfactory bulb neurons; Engel et al., 1996) with

$$g_{Kf} = g_{Kf,max} m^2 h$$

and

$$m_\infty = 1/(1 + \exp(-(U + 20)/15))$$

$$\tau_m = 3/(1 + 0.0009(U + 30)^2)$$

$$h_\infty = 1/(1 + \exp((U + 65)/15))$$

$$\tau_h = 50$$

4. Voltage- and Ca^{2+}-dependent K^+ current I_{BK} (modified current from cerebellar Purkinje cells; de Schutter and Bower, 1994) with

$$g_{BK} = g_{BK,max} m\, z^2$$

and

$$m_\infty = 7.5/(7.5 + 0.11/\exp((U - 50)/10))$$

$$\tau_m = 3\text{–}20/(7.5 + 0.11/\exp((U - 50)/10))$$

$$z_\infty = 1/(1 + 0.004[Ca^{2+}]_i)$$

$$\tau_z = 3$$

5. Small conductance Ca^{2+}-dependent K^+ current I_{SK}. The description of this current is a modified version of that for thalamic reticular neurons

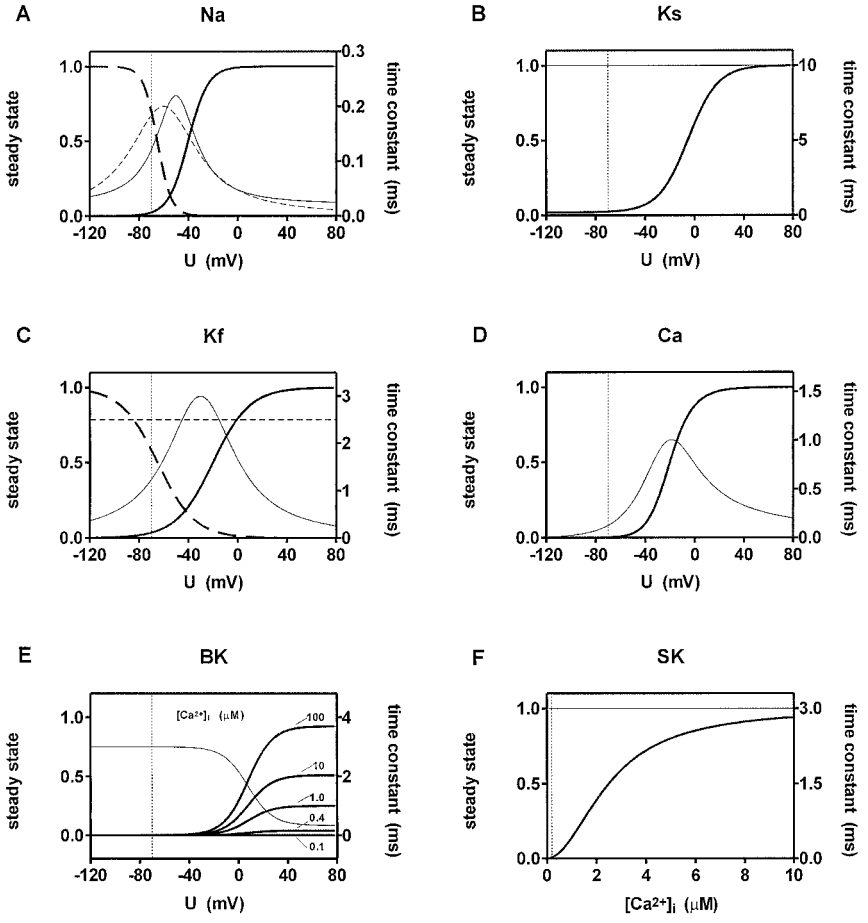

FIGURE 1 Activation (*heavy solid line*) and inactivation (*heavy dashed line*) curves and activation (*light solid line*) and inactivation (*light dashed line*) time constants of the ionic conductances used in the model. (*A*) Na^+ current, (*B*) slowly activating K^+ current, (*C*) fast-activating and -inactivating K^+ current, (*D*) high voltage-activated Ca^{2+} current, (*E*) voltage- and Ca^{2+}-dependent K^+ current, (*F*) small conductance Ca^{2+}-dependent K^+ current. Inactivation time constants were divided by 10 to fit in the same plot. The vertical dotted line indicates the resting values for membrane potential and $[Ca^{2+}]_i$, respectively.

(Destexhe et al., 1994) with the midpoint of the activation function $z([Ca^{2+}]_i)$ at 2.5 μM $[Ca^{2+}]_i$ instead of 25 μM. This was done because recent studies on SK channels, which corroborated the steep sigmoidal Ca^{2+}-dependent activation of the current, yielded lower $K_{1/2}$ values of 1 μM (Leinders and Vijverberg, 1992) and 0.4–0.7 μM $[Ca^{2+}]_i$ (Köhler et al., 1996), respectively. The discrepancy in the $K_{1/2}$ values may be explained by the fact that I_{AHP} (I_{SK}) can be inhibited by monoamine transmitters (norepinephrine, serotonin, histamine, dopamine) in a dose-dependent manner via protein kinases (Pedarzani and Storm, 1995). As the mechanisms of SK channel phosphorylation are unknown and phosphorylation could shift the channel's $[Ca^{2+}]_i$ sensitivity, we chose a midpoint value $K_{1/2}$ of 2.5 μM, which is between the reported values. In addition, a $K_{1/2}$ of 2.5 μM corresponds well to the half-maximum activation of the SK current in hair cells (2 μM $[Ca^{2+}]_i$) which was obtained by combined Ca^{2+} imaging and patch clamp measurements (Tucker and Fettiplace, 1996):

$$g_{SK} = g_{SK,max} z^2$$

and

$$z_\infty = ([Ca^{2+}]_i/0.0025)^2/(1 + ([Ca^{2+}]_i/0.0025)^2)$$

$$\tau_z = 3$$

6. High voltage-activated Ca^{2+} current I_{Ca}. The high voltage-activated calcium current was adapted from Hines' program cachan.mod added to the NEURON version 3.1.0, where the Goldman-Hodgkin-Katz permeability equation is used for the description of the driving force taking into account that influx of Ca^{2+} ions severely changes $[Ca^{2+}]_i$. From this arises the calcium current

$$I_{Ca} = P_{Ca,max} o^2 \Gamma(U, [Ca^{2+}]_i, [Ca^{2+}]_o),$$

with P being the maximum permeability of the Ca^{2+} channel, o the fraction of open channels, and $\Gamma(U, [Ca^{2+}]_i, [Ca^{2+}]_o)$ the driving force according to the Goldman-Hodgkin-Katz-equation that depends on voltage, external ($[Ca^{2+}]_o$), and the varying internal Ca^{2+} concentration ($[Ca^{2+}]_i$). $[Ca^{2+}]_o$ was set to 2 mM.

7. Ca^{2+} diffusion, buffering, and extrusion by a Ca^{2+} pump. Changes in $[Ca^{2+}]_i$ were accounted for only in the soma. The soma was subdivided into four concentric cylinders; only radial diffusion across these cylinders was calculated. They were filled homogenously with 250 μM of a Ca^{2+} buffer with a K_d of 10 μM (cf. Neher and Augustine, 1992) and a diffusion coefficient of 0.6 μm^2/ms (Hodgkin and Keynes, 1957). The free Ca^{2+} concentration in the outermost cylinder shell with a thickness of 0.75 μm was taken for the intracellular free Ca^{2+} concentration ($[Ca^{2+}]_i$). Ca^{2+} ions were extruded from the cell by a Ca^{2+} pump that in a first step bound an internal Ca^{2+} ion and in a second step translocated the ion and released it extracellularly:

$$\text{pump} + Ca_i^{2+} \leftrightarrow \text{pumpCa}$$

(with the rate constants k_1 and k_2)

$$\text{pumpCa} \leftrightarrow \text{pump} + Ca_o^{2+}$$

(with the rate constants k_3 and k_4).

The rate constants were $k_1 = 5 \cdot 10^8$ mM^{-1} s^{-1}, $k_2 = 2.5 \cdot 10^5$ s^{-1}, $k_3 = 5 \cdot 10^2$ s^{-1}, and $k_4 = 5$ mM^{-1} s^{-1}. The outward current produced by the pump was taken into account for the calculation of total calcium current and membrane potential.

Calculation of Ca^{2+} diffusion, buffering, and pumping was accomplished by combining and modifying Hines' programs cadifusl.mod and cabpump.mod that came along with NEURON version 3.1.0 (Hines, 1993).

Values for the maximum conductances used in the simulations were (S/cm^2): $g_{Na,max}$ = 0.6, $g_{Ks,max}$ = 0.0063 (soma), $g_{Ks,max}$ = 0.00063 (dendrites), $g_{Kf,max}$ = 0.03, $g_{BK,max}$ = 0.1, $g_{SK,max}$ = 0.04; maximum permeability $P_{Ca,max}$ = 0.0002 cm/s; concentration of the Ca^{2+} pump = 10^{-14} mol/cm^2.

RESULTS

Action potential shape, $[Ca^{2+}]_i$, and underlying currents

With the parameters given in Material and Methods, the neuron assumed a resting potential of −71 mV. Initial $[Ca^{2+}]_i$ was set to 200 nM. This value decreased slightly after the onset of the simulation because of the activity of the Ca^{2+} pump, but $[Ca^{2+}]_i$ never fell below 100 nM even at low spike frequency (>3 spikes/s). Current injection (5–200 pA) into the soma of the model neuron resulted in the generation of action potential trains with varying frequency. Fig. 2 shows a train of action potentials (*A*) and the underlying currents of two spikes selected from this spike train (*A* and *B*). It was elicited by sustained injection of 30 pA into the neuron. During the first spike, $[Ca^{2+}]_i$ increased from 118 nM to 536 nM (*C*, *solid line*), which was insufficient to substantially activate the Ca^{2+}-dependent K^+ currents (*E*). Sustained spiking of the cell led to an increase of mean $[Ca^{2+}]_i$ (*C*, *dashed line*) because Ca^{2+} influx through Ca^{2+} channels could not be balanced by the activity of the Ca^{2+} pump and buffering mechanisms. Thus, during

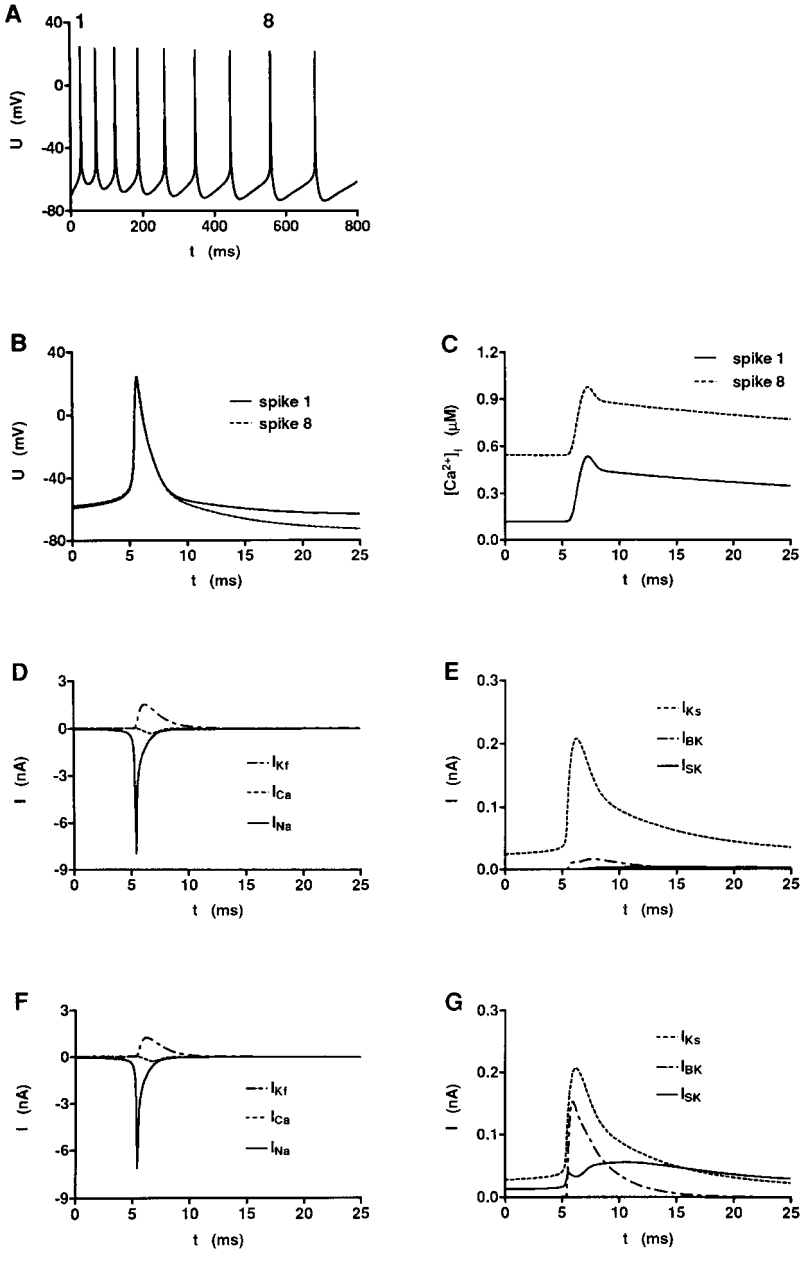

FIGURE 2 Comparison of two action potentials, underlying currents, and $[Ca^{2+}]_i$ increases elicited by sustained injection of 30 pA. The first and a later (8th) action potential selected from a train of APs (*A*) are superimposed in (*B*) and the respective $[Ca^{2+}]_i$ increases are shown in *C*. Underlying currents are depicted in *D* and *E* for the first AP and in *F* and *G* for the later one. In the first AP, the Ca^{2+}-dependent K^+ currents I_{BK} and I_{SK} were negligible (*E*) because $[Ca^{2+}]_i$ was initially very low. Spiking activity led to a rise in mean $[Ca^{2+}]_i$ that activated both I_{BK} and I_{SK} (*G*) in the later spike. I_{Kf}, I_{Ca}, and I_{Na} were little affected.

the later spike both I_{BK} and I_{SK} were activated (*G*) causing a pronounced and long-lasting hyperpolarization (*A* and *B*).

Spiking behavior without SK conductance

To investigate the role of SK channels in spike frequency adaptation, we first tested the spiking behavior of a model neuron without SK conductance. Fig. 3 shows four trains of APs evoked by sustained injection of 10–100 pA (*A–D*, *left*) as well as the respective traces for $[Ca^{2+}]_i$ (*A–D*, *right*). The frequency of APs in each AP train decreased slightly with time and reached a steady state (*A–C*) unless >95 pA were injected (*D*). In the latter case, the repolarizing mechanisms of the cell were insufficient to counteract the excitatory current. Instead the system fell into a new stationary state in which the cell had a membrane potential of −37 mV. Typically, g_{Na} was the predominant conductance in this steady state.

Spiking activity caused transient increases of $[Ca^{2+}]_i$ of ~420 nM per spike, and sustained spiking caused an increase in mean $[Ca^{2+}]_i$, i.e., the mean values of adjacent minima and maxima (see Fig. 3, *A–C*, *right column*), with time. For input currents >15 pA, corresponding to asymptotic spike rates ≥9 s^{-1}, mean $[Ca^{2+}]_i$ increased approximately linearly with time (Fig. 3, *B* and *C*). At input currents exceeding 95 pA, when the neuron had stopped firing and stayed depolarized at −37 mV, $[Ca^{2+}]_i$ increased linearly with time owing to the sustained voltage-dependent activation of the Ca^{2+} conductance and the resulting Ca^{2+} influx (Fig. 3 *D*).

To test the input-output relationship of the neuron without SK conductance, both asymptotic spike rate r_∞ (deter-

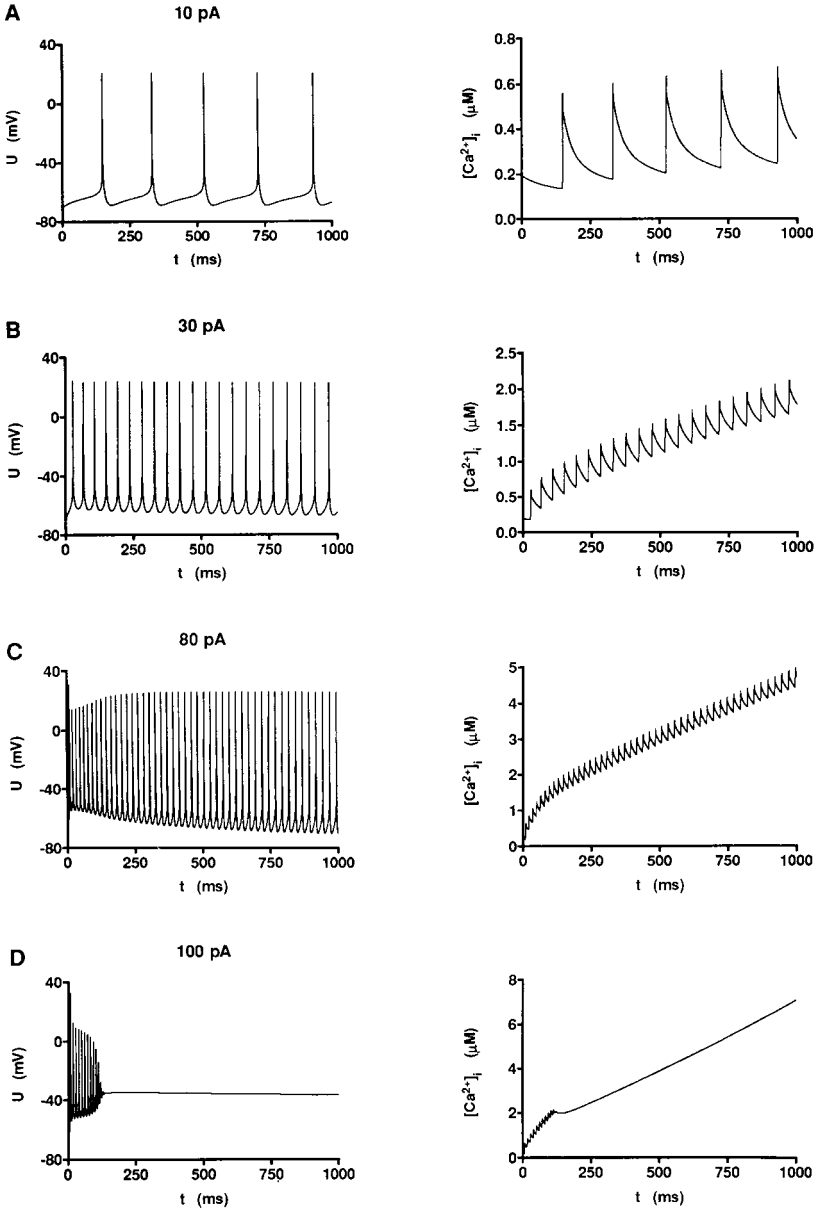

FIGURE 3 Spiking behavior of a model neuron that incorporates only the BK-type, but not the SK-type, Ca^{2+}-dependent K^+ conductance ($g_{BK,max}$ = 0.1 S/cm^2). Currents of different amplitudes indicated in the plots were continuously injected in the soma simulating synaptic input. The spike frequency reached a steady state (*left row*) unless the input current was too high, leaving the neuron depolarized at −37 mV (*D*, *left*). Mean $[Ca^{2+}]_i$ increased with time (*right*).

mined as the reciprocal of the time between the last two spikes at the end of the record) and the corresponding mean $[Ca^{2+}]_i$ were plotted as a function of the injected current (Fig. 4). The input range was limited by the cessation of firing, which in this case occurred above 95 pA. Both asymptotic spike frequency and $[Ca^{2+}]_i$ increased monotonically with increasing input current. In the case of $[Ca^{2+}]_i$, this relationship was linear ($r^2 = 0.9996$). In a first approximation, the asymptotic spike frequency could also be considered to be an almost linear function of the input ($r^2 = 0.972$), though it clearly shows a slight curvature.

SK conductance causes spike frequency adaptation and changes the transfer function

Having established the input-output relationship of a neuron with only the BK type of Ca^{2+}-dependent K^+ channels, we then analyzed the spiking properties of a neuron with an SK conductance ($g_{SK,max} = 0.04$ S/cm^2) (Fig. 5). The model neuron with g_{SK} responded to the same excitatory currents (10–100 pA) with considerably lower spike frequencies than that without g_{SK} (cf. Fig. 3). Moreover, it kept firing at 100 pA input current (*C*), an intensity that led to sustained depolarization in the neuron without g_{SK}. The SK conductance enabled the neuron to cope with input currents as large as 200 pA. Another striking difference was that for all input currents tested the mean $[Ca^{2+}]_i$ reached a constant value rather than increasing linearly with time. The right column of Fig. 5 shows the SK currents corresponding to the spike trains shown in the left column. Clearly, I_{SK} and g_{SK} activate during each spike and contribute to the repolarization of action potentials. In addition, and likewise importantly, g_{SK} increases to a steady state value between spikes similarly to $[Ca^{2+}]_i$.

The input-output relationship clearly demonstrates the effect of the SK conductance on the spiking properties (Fig. 6). Both asymptotic spike rate and asymptotic mean $[Ca^{2+}]_i$ could be described in good approximation as logarithmic functions of the input current (*A* and *B*). Plotting asymptotic mean $[Ca^{2+}]_i$ as a function of asymptotic spike rate revealed a virtually linear relationship with a small deviation at the smallest values of spike rate and $[Ca^{2+}]_i$. This suggests the interesting point that the mean level of $[Ca^{2+}]_i$ reflects the spiking activity of the neuron. In other words, the neuron "knows" its spike rate even during interspike intervals.

So far, the maximum specific SK conductance $g_{SK,max}$ was held constant at 0.04 S/cm^2. It was intriguing to see how spike frequency adaptation depended on this parameter. Fig. 7 shows the dependence of the initial (*A*) and the asymptotic (*B*) spike rate on the input current for different values of $g_{SK,max}$, including the case of $g_{SK,max} = 0$ (*uppermost curve*, *upright triangles*). Expectedly, the value of $g_{SK,max}$ had little effect on the dependence of the initial spike rate on I_{stim}, because the Ca^{2+} increase brought about by the first spike was too small to significantly activate the SK conductance and prolong the first interspike interval. However, $g_{SK,max}$ had a marked effect on the dependence of the asymptotic spike frequency on the input current (Fig. 7 *B*). On increasing $g_{SK,max}$ from 0 to 0.1 S/cm^2, the slope of the asymptotic rate transfer function decreased remarkably. When $g_{SK,max}$ was raised to 0.01 S/cm^2 or more, the asymptotic spike rate increased progressively less as a function of I_{stim} because of the massive negative feedback (short-circuit) exerted by the SK outward current on the input. In Fig. 7 *C* the degree of adaptation, i.e., the ratio between initial and asymptotic spike rate as a function of the input current, is shown for different maximum SK conductances. In general, the degree of adaptation had a sigmoidal dependence on the input and increased with increasing $g_{SK,max}$. The SK conductance had one more effect on the input-output characteristics in that it increased the input range the neuron could deal with Fig. 7 *D* shows the maximum input currents to which the cell responded with regular spiking as a function of $g_{SK,max}$. If higher input currents had been injected the neuron would have persisted in a depolarized state (Fig. 3 *D*). Increasing $g_{SK,max}$ from 0 to 0.4 S/cm^2 increased the input range by a factor of 2.5. For comparison, the respective asymptotic spike rates at maximum current injection are depicted in Fig. 7 *D*, which again demonstrates the efficient down-regulation of spike frequency by g_{SK}.

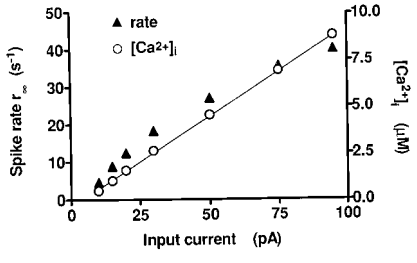

FIGURE 4 Steady-state spike frequency (r_∞) and respective mean $[Ca^{2+}]_i$ values as a function of the injected current in a model neuron with a BK-type Ca^{2+}-dependent K^+ conductance ($g_{BK,max} = 0.1$ S/cm^2). The spike frequency is in first approximation a linear function of the input current I_{stim}; mean $[Ca^{2+}]_i$ is a linear function of I_{stim}.

DISCUSSION

In this study we have modeled a standard Hodgkin-Huxley neuron with the voltage-gated conductances g_{Na}, g_{Ks}, and g_{Kf}. In addition, we inserted a high-voltage-activated calcium conductance g_{Ca}, modeled according to the Goldman-Hodgkin-Katz mechanism, as well as a BK-type Ca^{2+}-dependent potassium conductance g_{BK}. In models of this size many parameters have to be determined, and most of them have never been measured within one neuron, so we took the parameters from different neurons as stated in the Methods section. However, the choice of parameters is less crucial than might be assumed. Within the range where spiking occurs, parameter variations influence the shape of single APs, but they do not change the output spike rate as a function of the input current. This is because the time constants of activation, deactivation, inactivation, and re-

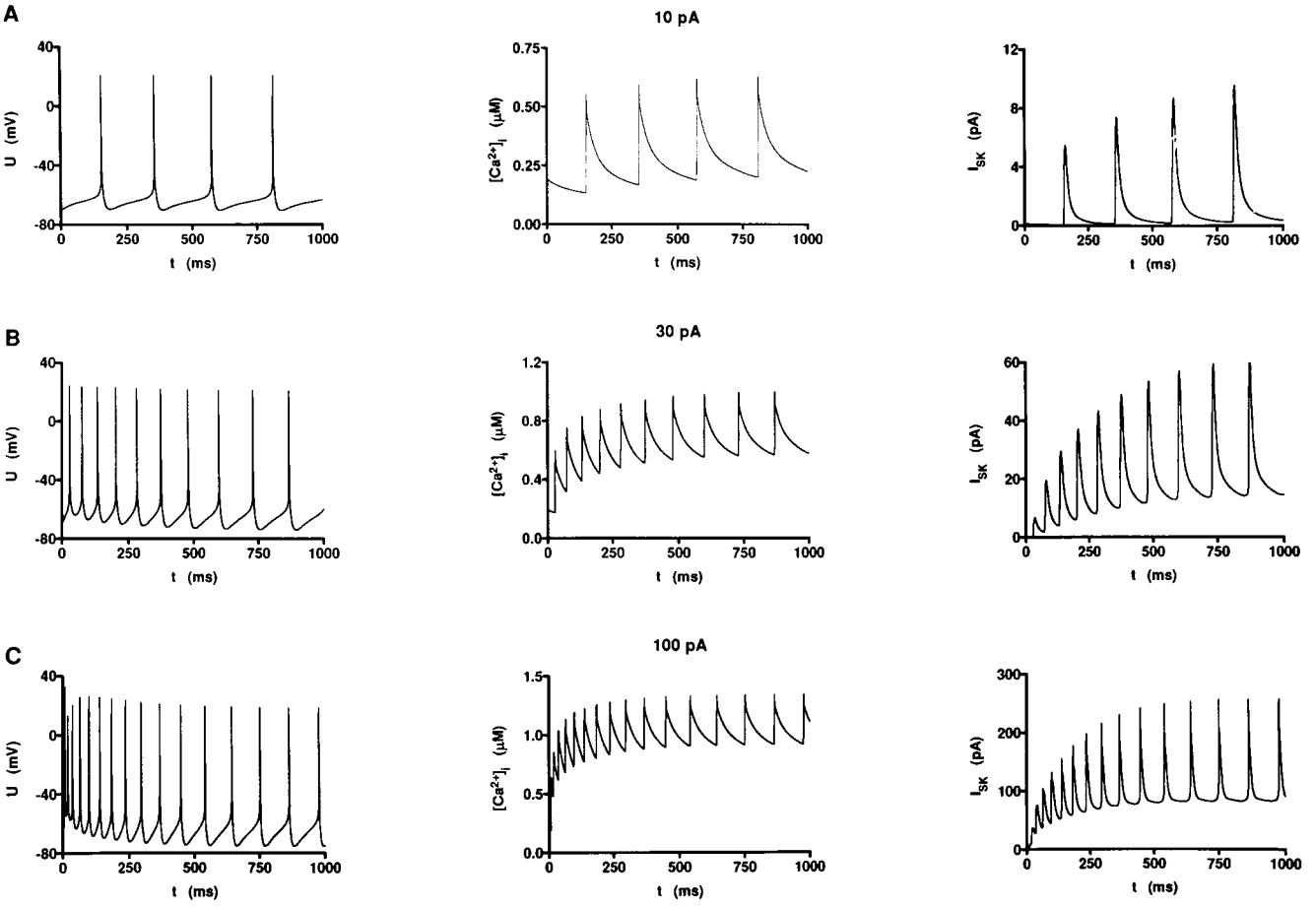

FIGURE 5 Spiking behavior of a model neuron that incorporates both a BK and an SK Ca^{2+}-dependent K^+ conductance ($g_{BK,max} = 0.1$ S/cm^2, $g_{SK,max} = 0.04$ S/cm^2). Voltage (*left*), $[Ca^{2+}]_i$ (*middle*), and SK current traces (*right*) are shown for three different input currents indicated in the plot (*upper*, *middle*, and *lower row*). Spike rate, mean $[Ca^{2+}]_i$, and interspike SK current reach a steady state.

moval of inactivation are all fast as compared to the relevant interspike intervals. The only system variable that is changed by action potentials for much longer a time than the voltage-dependent time constants is $[Ca^{2+}]_i$. This has, however, no effect at the resting voltage because the only Ca^{2+}-dependent conductance so far incorporated in the model (g_{BK}) is largely deactivated as a function of voltage. Taken together, the generation of a spike in the model lacking g_{SK} does not, in a first approximation, depend on the history of the spike train. For the sake of clarity we have therefore not shown the effects of parameter variations on the spike shape.

As the decisive step in our model we introduced an SK-type Ca^{2+}-dependent K^+ conductance. g_{SK} is activated by $[Ca^{2+}]_i$ and not by membrane voltage. This means that g_{SK} is activated as long as $[Ca^{2+}]_i$ is increased and that the history of a spike train, in particular $[Ca^{2+}]_i$ and g_{SK}, determine the membrane conductance at the onset of subsequent spikes. Because $[Ca^{2+}]_i$ as the leaky integral of Ca^{2+} influx is produced by the cell's output, i.e., spikes, and because the action of $[Ca^{2+}]_i$ upon g_{SK} subtracts the current I_{SK} from the input current, the remainder being the current that drives the spiking generator, this g_{Ca}-g_{SK} system forms a negative feedback circuit as shown in Fig. 8. This figure shows a schematic diagram of the model neuron together with the SK feedback circuitry. g_{Na}, g_{Ks}, g_{Kf}, and g_{BK} are depicted in the conventional way. The two transmembrane branches that are important for the feedback, i.e., g_{Ca} and g_{SK}, are shown on a larger scale. The operational amplifier OPA_1 measures the voltage drop u_{ICa} over $1/g_{Ca}$, which is proportional to I_{Ca}, and OPA_2 integrates u_{ICa} with a time constant $R_{load}C_{Ca}$. The Ca^{2+} buffering and extrusion mechanisms are lumped by making the integration of u_{ICa} leaky ($\tau_{leak} = R_{decay}C_{Ca}$). The leaky integration of the calcium influx leads to a voltage $u_{[Ca]}$ that is proportional to $[Ca^{2+}]_i$. This voltage modulates g_{SK}, thereby leading to a short-circuit of the membrane that is controlled by Ca^{2+}, and thus by the mean firing rate of the neuron.

Why does this negative feedback lead to an approximately logarithmic input-output relationship? While the underlying cellular mechanisms are as yet unknown, a tentative theoretical explanation can be given. In the range up to 10 μM, $[Ca^{2+}]_i$ increases about linearly with the spike rate if g_{SK} is zero. In the presence of g_{SK}, the dose-response curve g_{SK} ($[Ca^{2+}]_i$) has a sigmoidal shape (Leinders and Vijverberg, 1992; Köhler et al., 1996; Destexhe et al.,

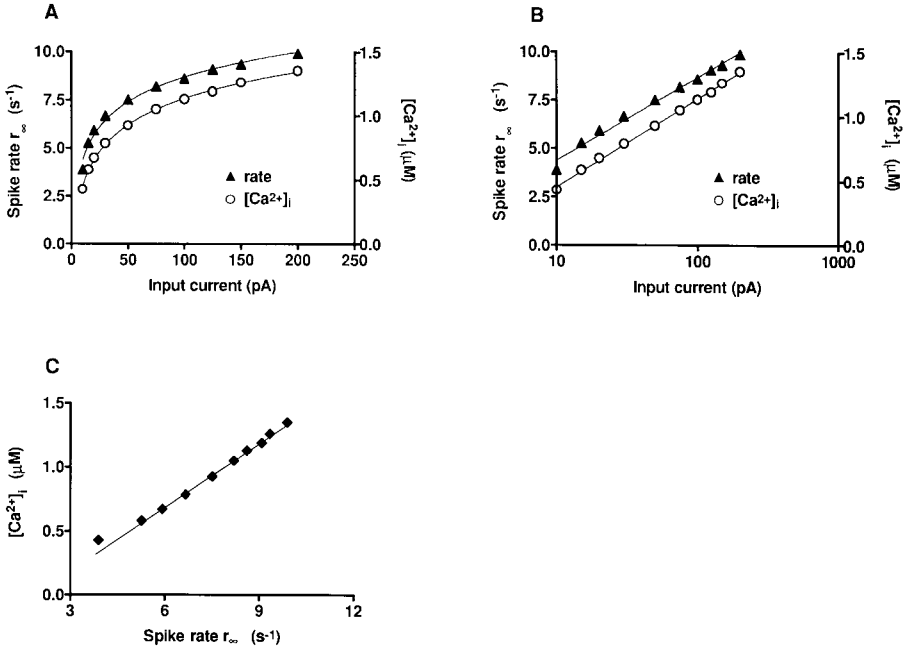

FIGURE 6 Steady-state spike frequency and respective $[Ca^{2+}]_i$ values as a function of the injected current in a model neuron with BK- and SK-type Ca^{2+}-dependent K^+ conductances ($g_{BK,max}$ = 0.1 S/cm^2, $g_{SK,max}$ = 0.04 S/cm^2). The SK conductance changed the transfer function of the neuron: both asymptotic spike rate (r_∞) and mean $[Ca^{2+}]_i$ became logarithmic functions of $I_{s\text{-}tim}$ (*B*). Mean $[Ca^{2+}]_i$ was proportional to the asymptotic spike rate (*C*).

1994), the left part of which can be approximated by an exponential, so that in a certain approximation the question becomes "how does an approximately linear system behave if an approximately exponential feedback is inserted?" The simple electronic analog would be an operational amplifier with a diode in the feedback branch. The diode characteristic can be approximated by an exponential. The output voltage u_o as a function of the input voltage u_i is then

$$u_o = A \cdot \log(u_i/u_c)$$

with A and u_c being calibration constants.

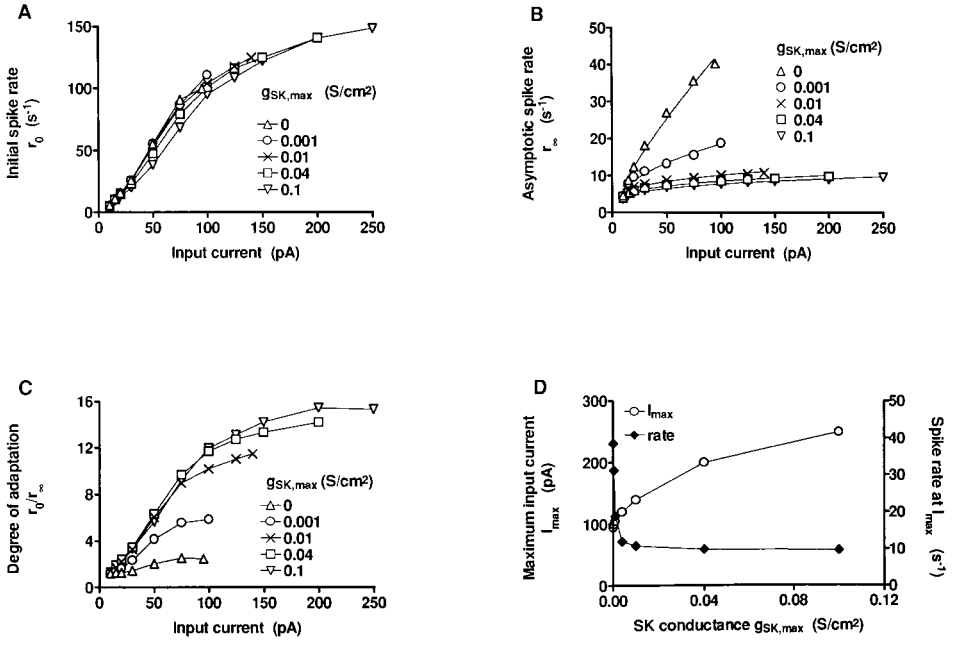

FIGURE 7 The amount of the SK-type Ca^{2+}-dependent K^+ conductance determines both the degree of spike frequency adaptation and the extent of the input range. Initial spike rates (*A*) and asymptotic spike rates (*B*) are shown as functions of the input current for different conductances $g_{SK,max}$ inserted in the model neuron. Increasing the maximum SK conductance of the neuron had a small effect on the initial spike rate, whereas the asymptotic spike rate was dramatically reduced at high input currents. Increasing values for $g_{SK,max}$ made adaptation more efficient, as depicted in (*C*), where the degree of adaptation, i.e., the ratio between initial and asymptotic spike frequency, is shown as a function of the input current. (*D*) $g_{SK,max}$ also determined the maximum input current the neuron responded to with regular spiking because of down-regulation of the spike frequency (*open symbols, left axis*). Also shown are the maximum asymptotic spike rates as a function of $g_{SK,max}$ (*closed symbols, right axis*).

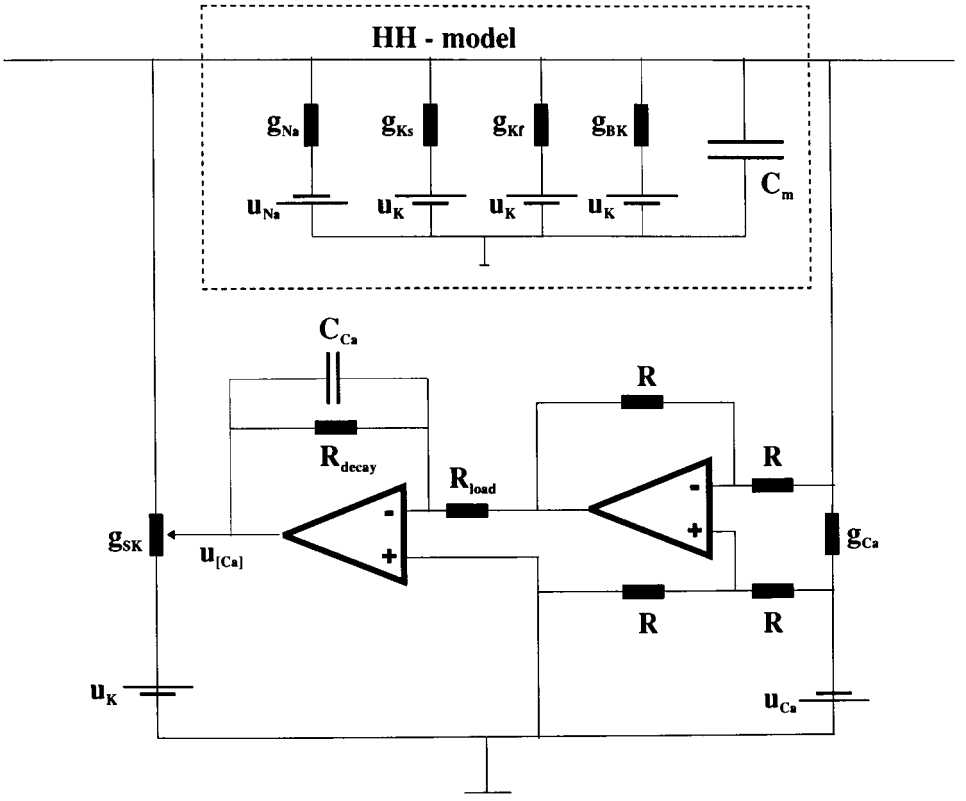

FIGURE 8 Equivalent circuit of the model neuron comprising the conductances g_{Na}, g_{Ca}, g_{Ks}, g_{Kf}, g_{BK}, and g_{SK}; u_i: Nernst potentials for ion species i. I_{Ca} is transformed to a voltage u_{Ca} which is then (leaky) integrated to give $u_{[Ca]}$, which is proportional to $[Ca^{2+}]_i$. $u_{[Ca]}$ controls the SK conductance and thereby exerts a feedback inhibition.

The approximations made in this explanation may be justified, because physiologically it may not be crucially important whether the spike rate is a logarithmic function or a power function with exponent 0.5 of the input current *I*.

Taken together, the nonlinearity of the sigmoidal activation curve $g_{SK}([Ca^{2+}]_i)$ is responsible for the logarithmic shape of the transfer functions. When the resting $[Ca^{2+}]_i$ is raised sufficiently by stimulation of the neuron, it reaches the concentration range where SK channels are activated, i.e., the left end of the dose-response curve ($g_{SK}([Ca^{2+}]_i)$), which is highly nonlinear (Leinders and Vijverberg, 1992; Köhler et al., 1996). In contrast, if the SK conductance depended in a linear way upon $[Ca^{2+}]_i$, the feedback as well as the overall transfer function would be linear, too (Wang, 1998).

Since the feedback mechanism essentially depends upon $[Ca^{2+}]_i$, it is of interest to test its sensitivity to changes in parameters that affect $[Ca^{2+}]_i$. We therefore varied the following parameters by two orders of magnitude while all others were held constant: Ca^{2+} channel permeability, number of Ca^{2+} pumps, Ca^{2+} buffer concentration, and the K_d of the Ca^{2+} buffer. Transfer functions were determined in the absence and presence of g_{SK} (not shown). Whenever spike activity shifted $[Ca^{2+}]_i$ in the neuron comprising g_{SK} to the nonlinear range of the dose-response curve of the SK channel, adaptational behavior, the change from (quasi-)linear to logarithmic transfer functions as well as an increase of the input range were observed. These effects did not occur in two cases where the parameter constellation prevented the activity-dependent increase in $[Ca^{2+}]_i$ to significantly activate g_{SK}. If, however, g_{SK} was fully activated by only a few spikes, the strong negative feedback exerted by it could prevent the neuron from further spiking.

The logarithmic relationship between input and output of the neuron obviously means two things: 1) Every neuron has an upper limit of its firing frequency. The more expressed an SK conductance is, the larger the input current that drives the neuron to this limit. This allows a relatively large range of input current that a neuron can deal with. 2) However, the sensitivity of the neuron ($\Delta r/\Delta I$), being highest for small input currents, decreases with larger input currents. This corresponds exactly to the psychophysical mechanism known as Fechner's law.

The last point to be mentioned here has little to do with the neuronal transfer function. Fig. 6 *C* shows that the mean $[Ca^{2+}]_i$ is related in an unambiguous way to the output (spike rate) of the neuron. Indeed, a linear relationship between mean $[Ca^{2+}]_i$ and spike rate has recently been measured in dendrites of pyramidal neurons (Helmchen et al., 1996). These cells were driven by repetitive current injection and the mean $[Ca^{2+}]_i$ reached a steady state after 0.5–1 s of regular (driven) spiking. This steady state would thus correspond to the adapted state of our model neuron. The linear relationship between mean $[Ca^{2+}]_i$ and spike rate is an interesting point because it means that the neuron has a system variable, i.e., the mean $[Ca^{2+}]_i$, that conveys information on the neuronal activity even during the interspike intervals. The time scale of cellular activity is thereby extended from that of single spikes to that of the decay constant of $[Ca^{2+}]_i$ and processes that are initiated in an

activity-dependent way may depend directly on the mean $[Ca^{2+}]_i$. Evidence for $[Ca^{2+}]_i$-controlled gene expression has in fact been reported (Roche and Prentki, 1994).

We are grateful to Michael Hines and Stefan Münkner for their help and stimulating discussions.

REFERENCES

Armstrong, C. M. 1992. Voltage-dependent ion channels and their gating. *Physiol. Rev.* 72:S5–S13.

Avoli, M., and A. Olivier. 1989. Electrophysiological properties and synaptic responses in the deep layers of the human epileptogenic neocortex in vitro. *J. Neurophysiol.* 61:589–606.

Bal, T., and D. A. McCormick. 1993. Mechanisms of oscillatory activity in guinea pig nucleus reticularis thalami in vitro: a mammalian pacemaker. *J. Physiol. (Lond.).* 469:669–691.

Barret, J. N., K. L. Magleby, and B. S. Palotta. 1982. Properties of single calcium-activated potassium channels in cultured rat muscle. *J. Physiol. (Lond.).* 331:211–230.

Blatz, A. L., and K. L. Magleby. 1986. Single apamin-blocked Ca-activated K^+ channels of small conductance in cultured rat skeletal muscle. *Nature.* 323:718–720.

Blatz, A. L., and K. L. Magleby. 1987. Calcium-activated potassium channels. *TINS.* 10:463–467.

Connors, B. W., R. C. Malenka, and L. R. Silva. 1988. Two inhibitory postsynaptic potentials, and GABAA and GABAB receptor-mediated responses in neocortex of rat and cat. *J. Physiol. (Lond.).* 406:443–468.

de Schutter, E., and J. M. Bower. 1994. An active membrane model of the cerebellar Purkinje cell. I. Simulation of current clamps in slice. *J. Neurophysiol.* 71:375–400.

Destexhe, A., D. Contreras, T. J. Sejnowski, and M. Steriade. 1994. A model of spindle rhythmicity in the isolated thalamic reticular nucleus. *J. Neurophysiol.* 72:803–818.

Engel, J., J. Rabba, and D. Schild. 1996. A transient, RCK4-like K^+ current in cultured *Xenopus* olfactory bulb neurons. *Pflügers Arch.* 432:845–852.

Helmchen, F., K. Imoto, and B. Sakman. 1996. Ca^{2+} buffering and action potential-evoked Ca^{2+} signaling in dendrites of pyramidal neurons. *Biophys. J.* 70:1069–1081.

Hille, B. 1992. Ionic channels of excitable membranes, 2nd Ed. Sinauer Associates Inc., Sunderland, MA.

Hines, M. 1993. NEURON—a program for simulation of nerve equations. *In* Neural Systems: Analysis and Modeling. F. Eeckman, editor. Kluwer Academic Publishers, Norwell, MA. 127–136.

Hodgkin, A. L., and A. F. Huxley. 1952. A quantitative description of membrane current and its application to conduction and excitation in nerve. *J. Physiol. (Lond.).* 117:500–544.

Hodgkin, A. L., and R. D. Keynes. 1957. Movements of labelled calcium in squid giant axons. *J. Physiol. (Lond.).* 138:253–281.

Köhler, M., B. Hirschberg, C. T. Bond, J. M. Kinzie, N. V. Marrion, J. Maylie, and J. P. Adelman. 1996. Small-conductance, calcium-activated potassium channels from mammalian brain. *Science.* 273:1709–1714.

Koike, H., N. Mano, Y. Okada, and T. Oshima. 1970. Repetitive impulses generated in fast and slow pyramidal cells by intracellularly applied current steps. *Exp. Brain. Res.* 11:263–281.

Lancaster, B., and R. A. Nicoll. 1987. Properties of two calcium-activated hyperpolarizations in rat hippocampal neurones. *J. Physiol. (Lond.).* 389:187–203.

Lanthorn, T., J. Storm, and P. Andersen. 1984. Current-to-frequency transduction in CA1 hippocampal pyramidal cells: slow prepotentials dominate the primary range firing. *Exp. Brain Res.* 53:431–443.

Leinders, T., and H. P. M. Vijverberg. 1992. Ca^{2+} dependence of small Ca^{2+}-activated K^+ channels in cultured N1E-115 mouse neuroblastoma cells. *Pflügers Arch.* 422:223–232.

Madison, D. V., and R. A. Nicoll. 1984. Control of the repetitive discharge of rat CA1 pyramidal neurons in vitro. *J. Physiol. (Lond.).* 354:319–331.

Mason, A., and A. Larkman. 1990. Correlations between morphology and electrophysiology of pyramidal neurons in slices of rat visual cortex. II. Electrophysiology. *J. Neurosci.* 10:1415–1428.

McManus, O. B., and K. L. Magleby. 1988. Kinetic states and modes of single large-conductance calcium-activated potassium channels in cultured rat skeletal muscle. *J. Physiol. (Lond.).* 402:79–120.

Neher, E., and G. J. Augustine. 1992. Calcium gradients and buffers in bovine chromaffin cells. *J. Physiol. (Lond.).* 450:273–301.

Pedarzani, P., and J. F. Storm. 1995. Dopamine modulates the slow Ca^{2+}-activated K^+ current I_{AHP} via cyclic AMP-dependent protein kinase in hippocampal neurons. *J. Neurophysiol.* 74:2749–2753.

Roche, E., and M. Prentki. 1994. Calcium regulation of immediate-early response genes. *Cell Calcium.* 16:331–338.

Schild, D. 1989. Whole-cell currents in olfactory receptor cells of *Xenopus laevis. Exp. Brain Res.* 78:223–232.

Tucker, T. R., and R. Fettiplace. 1996. Monitoring calcium in turtle hair cells with a calcium-activated potassium channel. *J. Physiol. (Lond.).* 494:613–626.

Wang, X.-J. 1998. Calcium coding and adaptive temporal computation in cortical pyramidal neurons. *J. Neurophysiol.* 79:1549–1566.

Wang, X. Y., J. S. McKenzie, and R. E. Kemm. 1996. Whole-cell K^+ currents in identified olfactory bulb output neurones of rats. *J. Physiol. (Lond.).* 490:63–77.

Zhou, F.-M., and J. J. Hablitz. 1996. Layer I neurons of rat neocortex. I. Action potential and repetitive firing properties. *J. Neurophysiol.* 76: 651–667.